Applied Catalysis B: Environmental 325 (2023) 122344

Contents lists available at ScienceDirect

Applied Catalysis B: Environmental

journal homepage: www.elsevier.com/locate/apcatb

Incorporation of atomically dispersed cobalt in the 2D metal–organic framework of a lamellar membrane for highly efficient peroxymonosulfate activation

Chao Yang [a], Shanshan Shang [a], Yiang Fan [a], Kaimin Shih [a], Xiao-yan Li [a,b,*], Lin Lin [b,**]

[a] Environmental Engineering Research Centre, Department of Civil Engineering, The University of Hong Kong, Pokfulam, Hong Kong, China
[b] Institute of Environment and Ecology, Tsinghua Shenzhen International Graduate School, Tsinghua University, Shenzhen, China

ARTICLE INFO

Keywords:
MOFs
Advanced oxidation processes
Membranes
Single-atom catalyst
Wastewater treatment

ABSTRACT

The peroxymonosulfate (PMS)-based Fenton-like reaction is one of the most promising technologies for controlling emerging organic pollutants in water and wastewater. Herein, we present a novel lamellar membrane comprised of a water-stable two-dimensional (2D) porphyrin metal–organic framework with atomically dispersed CoN_4 catalytic centers (Co_{SA}-PMOF) for highly efficient PMS activation. The single Co atoms decorating the porphyrin rings of Co_{SA}-PMOF boosted PMS activation and, subsequently, $SO_4^{\bullet-}$ radical generation. Co_{SA}-PMOF enhanced the degradation rate of moxifloxacin (MOX) in water by more than 20 times compared with the pristine PMOF. The novel 2D Co_{SA}-PMOF lamellar membrane achieved an exceptional performance, with 100 % MOX removal via single-pass filtration at a high flux of 48 L m^{-2} h^{-1}. Its excellent catalytic performance may be attributed to the confinement effect that traps PMS and pollutant molecules in the vicinity of the single-atom Co sites within the lamellar membrane during filtration.

1. Introduction

The presence of persistent emerging organic pollutants, such as pharmaceuticals, in wastewater poses serious risks to human health and aquatic environments [1]. For the removal of emerging organic pollutants, such as antibiotic moxifloxacin (MOX), advanced water and wastewater treatment technologies have been reported, including adsorption [2], membrane filtration [3], and advanced oxidation processes (AOPs) [4]. AOPs are among the most effective technologies for the removal of emerging organic pollutants, which are based on the generation of highly reactive radicals [5,6]. Recently, peroxymonosulfate (PMS)-based Fenton-like processes for advanced wastewater treatment have drawn increasing attention because of their advantages over the conventional hydrogen peroxide (H_2O_2)-based Fenton process, which include a strong oxidation capacity over a wide pH range, the generation of sulfate radicals ($SO_4^{\bullet-}$) with a long half-life, and environmental compatibility (i.e., little sludge generation) [7,8]. Although the homogeneous catalyst of Co^{2+} ions is highly reactive, its use is complicated by problems such as heavy metal pollution, sensitivity to reaction conditions, and difficulty in separation for reuse [9,10]. Using heterogeneous catalysts may overcome these limitations [11,12]. Accordingly, intensive research has been conducted on the development of efficient and sustainable heterogeneous catalysts for PMS activation to degrade emerging organic pollutants in the context of wastewater treatment and reuse [13,14].

Great efforts have been made to develop heterogeneous catalysts containing Co(II) species in nanoparticles for the activation of PMS, such as cobalt oxides, cobalt phosphates, spinel cobalt-ferrite, and catalysts on porous supports [15–21]. However, large amounts of active metal are embedded under the surfaces of these catalysts and are thus wasted, reducing the efficiency of PMS activation [22,23]. Thus, it is highly desirable to design and construct catalysts containing well-dispersed active sites with molecular precision to maximize the active-site exposure. Atomically dispersed metal active centers (hereafter, single-atom catalysts (SACs)) have attracted much attention in the field of catalysis owing to their ability to maximize metal utilization; thus, SACs are expected to bridge the gap between homogeneous and heterogeneous catalysts [22,24]. When fabricating SACs, coordinatively unsaturated

* Corresponding author at: Environmental Engineering Research Centre, Department of Civil Engineering, The University of Hong Kong, Pokfulam, Hong Kong, China.
** Corresponding author.
E-mail addresses: xlia@hku.hk (X.-y. Li), linlin00@sz.tsinghua.edu.cn (L. Lin).

https://doi.org/10.1016/j.apcatb.2022.122344
Received 18 October 2022; Received in revised form 15 December 2022; Accepted 28 December 2022
Available online 29 December 2022

sites in the support materials are a crucial component, as these sites anchor individual metal atoms and maintain the high dispersion of single atoms [25]. To date, metal oxides and carbon materials with defects have been used to stabilize single atoms in catalysts [26]. Compared with metal oxides and carbon materials, metal–organic frameworks (MOFs) demonstrate advantages in decorating single-atom catalysts. The unique structural diversity and designable properties of MOFs enable easy control of the catalytic sites at atomic precision. Meanwhile, MOFs as support can provide a large surface area for anchoring a large number of SAC centers for PMS activation.

Metal–organic frameworks (MOFs), which use metal atoms as the nodes and organic ligands as the linkers, have well-defined structures and ultrahigh surface areas and are increasingly used as supporting materials for heterogeneous catalysts in catalytic reactions and AOPs [27,28]. For instance, reports have described the application of the classic MOFs MIL-101(Fe) and MIL-53(Fe) for H_2O_2 activation [29,30], and ZIF-67, which uses Co as the metal node, has been applied to activate PMS for pollutant degradation [31]. Despite these great potential opportunities, the catalytic centers in existing MOFs for AOPs are derived mainly from the metal nodes (i.e., metal clusters) [32], which have poor structural stability in water. Recently, MOFs-based SACs showed a great potential for water treatment applications [33]. Due to their high porosity, high specific surface area, high structural diversity, and designable features, MOFs are excellent precursor materials for the preparation of dispersed single-atom catalysts. Currently, MOF-based SACs are mainly prepared by the high-temperature pyrolysis of MOF precursors [34,35]. However, there are still problems with the MOFs-based SACs, such as low catalyst yield, high cost, and low structural integrity [36]. Construction of highly effective and hydrolytically stable SACs on MOFs for water and wastewater treatment remains a daunting challenge [37,38].

The sustainable reuse of catalysts is another challenge associated with PMS activation. PMS activation processes are usually carried out in batch mode using powder catalysts [39]. For large-scale applications, the separation and recovery of powder catalysts after the reaction can be difficult and costly. Immobilization of the catalysts in water without compromising their contact with water is desired. To achieve this, one promising approach involves the assembly of 2D catalytic materials such as graphene oxide and MoS_2 into a lamellar membrane, which would allow water to flow continuously through the interlayer space between nanosheets of the catalysts [40,41]. Moreover, the spatial confinement effect in the lamellar membrane would facilitate mass transport and enhance the contact between the catalytic active sites and the aqueous-phase oxidants and pollutants for rapid catalytic oxidation. Although porphyrin-based MOF has been developed for gas adsorption and catalysis, it has not been designed and utilized for PMOF-based lamellar membrane with a single-atom catalyst for AOPs. The porphyrin ring in the MOF contains four pyrrolic nitrogen atomic sites in a square planar geometry, which provides a perfect site for capturing and stabilizing a single metal atom. The 2D nanosheet structure allows the SAC active sites to be fully exposed for catalytic reactions in water. It is a promising approach to decorate single-atom Co in the editable porphyrin ring structure of PMOF for PMS activation. The 2D Co_{SA}-PMOF can be further assembled into a lamellar membrane as a novel catalytic filter for continuous-flow wastewater treatment.

In this research, we synthesized a water-stable, two-dimensional (2D), porphyrin-based MOF (PMOF) for decorating single-atom Co(II) sites in an editable porphyrin ring structure (Co_{SA}-PMOF) as a SAC for PMS activation. The 2D Co_{SA}-PMOF can be readily assembled into a lamellar membrane via vacuum filtration. Using the 2D Co_{SA}-PMOF lamellar membrane as a novel catalytic filter for high-rate wastewater treatment via single-pass filtration, we demonstrated an excellent performance of the novel SAC and its lamellar membrane in the activation of PMS and degradation of the antibiotic moxifloxacin (MOX), a model organic pollutant, in synthetic wastewater. Realization of the redox cycle of Co(II)/Co(III) in the porphyrin center for PMS activation provides the Co_{SA}-PMOF membrane with excellent stability and reusability.

2. Experimental

2.1. Chemicals and reagents

PMS ($KHSO_5{\cdot}0.5\ KHSO_4{\cdot}0.5K_2SO_4$) and cobalt acetate were purchased from Aladdin (China). 4,4′,4′,4′-(Porphine-5,10,15,20-tetrayl) tetrakis (benzoic acid) (H_2TCPP), aluminum chloride hexahydrate ($AlCl_3{\cdot}6H_2O$), moxifloxacin (MOX), p-benzoquinone (pBQ), furfuryl alcohol (FFA), 5,5-dimethyl-1-pyrroline-N-oxide (DMPO), and 2,2,6,6-tetramethylpiperidine (TEMP) were obtained from Sigma-Aldrich (USA). Other chemicals and solvents were purchased from Merck (Germany). Deionized (DI) water (Milli-Q water, 18.2 MΩ cm) was used for the experiments.

2.2. Preparation of PMOF and Co_{SA}-PMOF

PMOF was synthesized using a hydrothermal method as previously reported with some modifications [42], including the use of aluminum and H_2TCPP as the metal node and ligand, respectively. (see details in Text S1, Supporting information). Atomically decorated PMOF (Co_{SA}-PMOF) was prepared using a post-synthetic modification method in dimethylformamide (DMF), in which the transition metal Co was inserted into the porphyrin rings of PMOF to form Co-N_4 sites. Specifically, the as-prepared PMOF (0.1 mmol) was added to DMF (25 mL) containing cobalt acetate (0.2 mmol). The solution was stirred for 20 min and then transferred into a 50 mL Teflon-lined autoclave and reacted at 120 °C for 48 h. The product was collected with filtration and washed thoroughly with DMF and acetone to remove the unreacted metal ions. Finally, Co_{SA}-PMOF was dried in a vacuum oven at 120 °C to remove the trapped guest molecules.

2.3. Fabrication of the self-assembled 2D Co_{SA}-PMOF lamellar membrane

A precursor solution was first prepared by dispersing Co_{SA}-PMOF (10 mg) into deionized (DI) water (50 mL), and then bath-sonicated for 2 h. The above dispersion was then diluted to 10 mg L^{-1} with DI water along with sonication for 10 min before filtration and membrane formation. The 2D MOF lamellar membrane with a diameter of 40 mm was fabricated through self-assembly via deposition of the Co_{SA}-PMOF catalyst on the indicated porous backing substrate (PVDF or Al_2O_3 ceramic membrane) through vacuum filtration of the catalyst suspension (10 mg L^{-1}). Catalyst loading (mg cm^{-2}) was controlled by varying the volume of the catalyst suspension to be filtered. The self-assembled Co_{SA}-PMOF membranes were dried in an oven at 60 °C overnight and then stored in a vacuum desiccator before use. The PMOF lamellar membrane was prepared using the same procedure for comparison.

2.4. Experimental test of catalytic activity

In a typical batch experiment, the as-prepared catalyst (0.1 g L^{-1}) was dispersed into a MOX solution (10 μM) at neutral pH. The reaction temperature was maintained at 25 °C. After reaching adsorption–desorption equilibrium, PMS was added to the MOX solution, and stirring was maintained throughout the experiment. During the test, 1-mL aliquots of the reaction solution were sampled at pre-determined time intervals and immediately quenched with 1 mM sodium thiosulphate to terminate the reaction. For more comprehensive evaluations, MOX degradation experiments were also conducted at different PMS dosing concentrations (0.25–1 mM) and in the presence of various ions.

Experiments to assess the catalytic performance of the 2D Co_{SA}-PMOF membrane were conducted in a continuous single-pass filtration mode. Synthetic wastewater containing MOX (10 μM) and PMS (0.5

mM) was pressurized to flow through the 2D Co_{SA}-PMOF membrane at a flow rate of 1 mL min^{-1}, corresponding to a flux of 48 L m^{-2} h^{-1} (LMH). During the tests, the treated permeate water was sampled at predetermined time intervals to evaluate the MOX degradation efficiency.

2.5. Characterization

The crystal structure of the catalysts was characterized by their powder X-ray diffraction (XRD) patterns using a Bruker D8 Advance diffractometer. The morphology of the catalyst materials was examined using the scanning electron microscopy (SEM, Hitachi S-4800) and transmission electron microscopy (TEM, FEI, Tecnai G2 20 S-TWIN) equipped with an energy-dispersive X-ray spectroscope (EDS). Aberration-corrected high-angle annular dark-field imaging (HAADF)-scanning TEM (HAADF-STEM) was performed on a JEOL JEM-ARM300F microscopy. The atomic force microscopy (AFM) images were obtained using a Bruker Dimension Icon AFM. N_2 adsorption-desorption experiments were performed on a Micromeritics 3Flex analyzer with liquid nitrogen (77 K) to measure the surface area and pore size distribution. The chemical composition of the samples was analyzed by the X-ray photoelectron spectroscopy (XPS, Thermo Scientific, ESCALAB 250Xi) with the binding energy calibrated with C 1s at 284.6 eV. An UV–visible spectrophotometer (Biochrom Libra S12) was used to identify the change of the chemicals in porphyrin structure. The electron paramagnetic resonance (EPR) spectra of the reaction systems were obtained with a Bruker EPR A300 spectrometer at room temperature. The X-ray absorption spectra (XAS) including X-ray absorption near-edge structure (XANES) and extended X-ray absorption fine structure (EXAFS) of the samples at Co K-edge were collected at the Singapore Synchrotron Light Source (SSLS) center in a transmission mode.

2.6. Analytical methods

The concentrations of MOX in the samples were determined by the high-performance liquid chromatography (HPLC, Waters e2695) equipped with a C18 column (4.6 mm × 250 mm × 5 μm) and a UV–vis photodiode array detector. The intermediate products of MOX degradation were identified by the liquid chromatography–quadrupole time-of-flight mass spectrometry (LC-QTOF-MS) (Agilent UPLC 1290-QTOF 6550). The active species during PMS activation were detected by the EPR analysis using DMPO, DMPO/DMSO, and TEMP as the trapping agents.

3. Results and discussion

3.1. Preparation and characterization of the Co_{SA}-PMOF catalyst

The 2D Co_{SA}-PMOF catalyst was constructed by decorating the PMOF with atomically dispersed CoN_4 as the active sites for PMS activation and subsequent catalytic organic oxidation. Fig. 1 illustrates the procedures of PMOF synthesis and atomically precise Co(II) decoration [42]. First, the PMOF was synthesized using porphyrin (H_2TCPP, with four pyrrolic nitrogen sites in a square-planar geometry) as the ligand and Al as the metal nodes. Second, Co_{SA}-PMOF was synthesized via post-synthesis modification through a solvothermal reaction. Specifically, Co(II) was inserted into the planar porphyrin rings of the PMOF, where it bound strongly to the N atoms to form atomically dispersed Co sites in the Co_{SA}-PMOF nanosheets.

In Fig. 2a, a scanning electron microscopy (SEM) image of Co_{SA}-PMOF shows a 2D nanosheet-type structure, which is consistent with the morphology of pristine PMOF (Fig. 2b). The X-ray diffraction (XRD) pattern of Co_{SA}-PMOF shows two characteristic diffraction peaks at 7.6° and 13.6° (Fig. 2c), which are also consistent with those of the pristine PMOF and indicate the good integrity and crystallinity of Co_{SA}-PMOF after Co-N_4 decoration [43]. The absence of diffraction peaks from metallic Co nanoparticles or Co oxides excludes the possibility that these impurities were formed and present in the catalyst. In Fig. 2d, the transmission electron microscopy (TEM) image confirms that the as-prepared Co_{SA}-PMOF had a homogeneous 2D nanosheet structure without nanoparticles, consistent with the XRD results. Using atomic force microscopy (AFM), the thickness of Co_{SA}-PMOF was determined to be around 4 nm (Fig. 2e). In addition, the Brunauer–Emmett–Teller (BET) surface area of Co_{SA}-PMOF, as measured by N_2 adsorption at 77 K, was similar to that of the PMOF (Fig. 2f), with a specific surface area in the range of 1304–1486 m^2 g^{-1} and a pore size distribution of 5–12 Å (Fig. S1, Supporting Information), suggesting a well-preserved porous structure. The percentage of single Co atoms in Co_{SA}-PMOF was determined quantitatively by inductively coupled plasma optical emission spectroscopy (ICP-OES) to be 6.1 wt. %.

3.2. Determination of the atomically decorated Co(II) sites

To characterize the unique structure of Co_{SA}-PMOF, its electronic properties were investigated using X-ray photoelectron spectroscopy (XPS) and UV-Vis spectroscopy. According to XPS analysis of the elemental composition (Table S1), the atomic content of Co was 1.90 a.t.

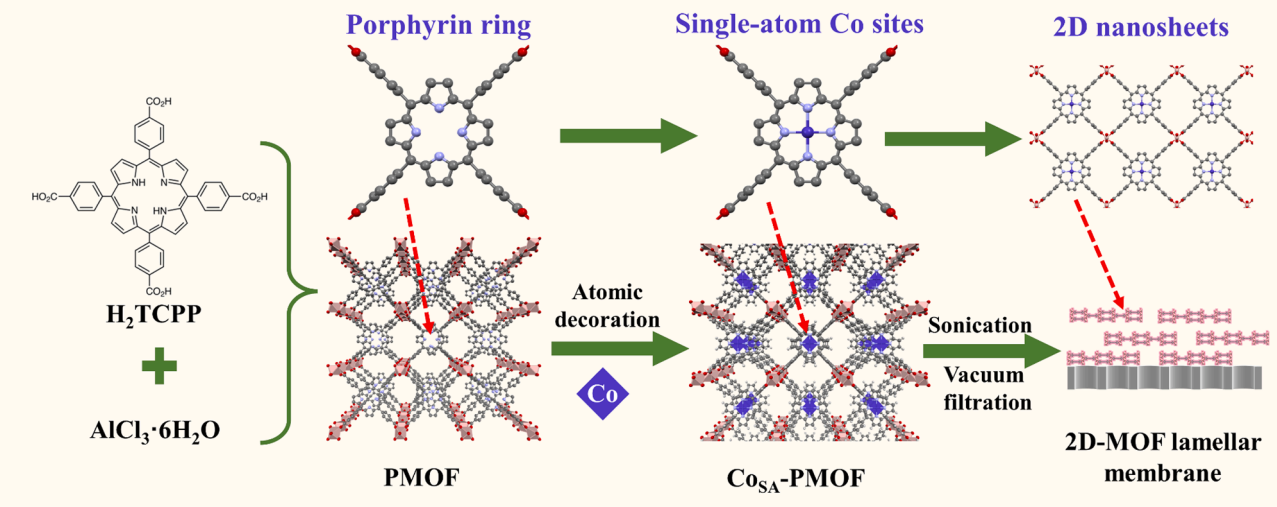

Fig. 1. Synthesis of the Co_{SA}-PMOF catalyst with atomically dispersed CoN_4 in the porphyrin rings, and self-assembly of the catalyst to form the 2D Co_{SA}-PMOF lamellar membrane.

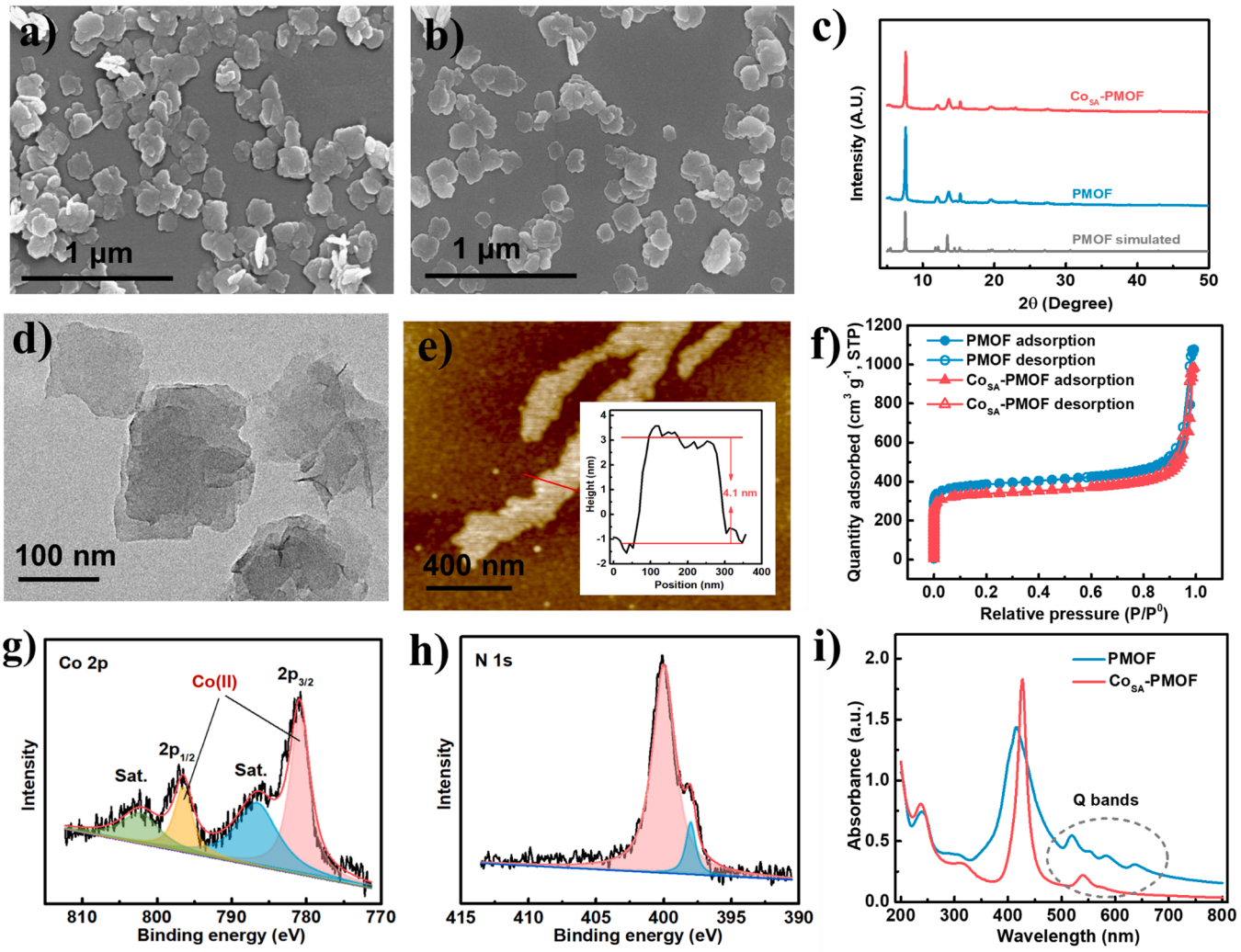

Fig. 2. Characterization of the catalyst materials: SEM images of (a) Co_{SA}-PMOF and (b) PMOF; (c) XRD patterns of Co_{SA}-PMOF and PMOF; (d) TEM and (e) AFM images of Co_{SA}-PMOF; (f) N_2 adsorption–desorption isotherms at 77 K of Co_{SA}-PMOF and PMOF; (g) XPS Co 2p and (h) N 1s spectra of Co_{SA}-PMOF; and (i) UV-Vis spectra of Co_{SA}-PMOF and PMOF.

% in the Co_{SA}-PMOF sample. The peaks at 781.1 eV and 796.5 eV in the XPS Co 2p spectrum of Co_{SA}-PMOF were assigned to Co(II) (Fig. 2g), and no metallic Co(0) species were observed [44]. The N 1 s spectrum of Co_{SA}-PMOF in Fig. 2h indicates that nitrogen existed predominantly in the form of pyrrolic N (399.9 eV), which typically serves as an anchoring point for Co atoms [45]. UV-Vis spectroscopy was used to confirm the local environment of porphyrin in the PMOF (Fig. 2i). Specifically, the decreased number of Q bands in Co_{SA}-PMOF (two) in comparison with the PMOF (four) resulted from the increase in symmetry after metal insertion, indicating the successful and atomically precise decoration of the porphyrin rings of the PMOF with Co atoms having a single-electron redox capacity [42].

The atomically dispersed Co sites in Co_{SA}-PMOF are further confirmed, as no obvious agglomeration of Co atoms can be observed in the high-resolution TEM image in Fig. 3a. The existence of single Co atoms was well supported by the results of aberration-corrected high-angle annular dark-field scanning transmission electron microscopy (HAADF-STEM). As shown in Fig. 3b, the bright spots (marked by red circles) corresponding to single Co atoms can be clearly observed, and the spatial distance between adjacent Co atoms in Co_{SA}-PMOF appears to have been finely controlled. Energy-dispersive X-ray spectroscopy (EDX) mapping of Co_{SA}-PMOF revealed the homogeneous distribution of Co and N species (Fig. 3c). X-ray absorption spectroscopy (XAS) analysis, including X-ray absorption near-edge structure (XANES) and extended X-ray absorption fine structure (EXAFS), was used to acquire additional atomic structural information about Co_{SA}-PMOF. As shown in Fig. 3d, Co K-edge XANES revealed that the rising edge for Co_{SA}-PMOF was situated at the same position as cobalt phthalocyanine (CoPc) and CoO, indicating the presence of Co atoms with an oxidation state of Co(II) in Co_{SA}-PMOF, which is consistent with the XPS results.

The Fourier-transformed (FT) EXAFS spectrum for Co_{SA}-PMOF shows a primary peak at 1.46 Å, which is assigned to the scattering path of Co-N (Fig. 3e). Compared with Co foil and CoO, no Co-Co coordination (2.1 Å) was observed in the spectrum of Co_{SA}-PMOF, indicating the atomic dispersion of Co in PMOF. The EXAFS spectrum was well-fitted, using the scattering path of Co-N from the cobalt porphyrin structure. The fitting results (Table S2, Supporting Information) revealed that the first shell of the Co atoms in Co_{SA}-PMOF possessed a Co-N coordination number of 4 (CoN_4 configuration). Wavelet transform (WT)-EXAFS analysis was performed to provide both R- and k-space information and discriminate the backscattering atoms. Co_{SA}-PMOF yielded a WT maximum at 4.5 Å^{-1}, corresponding to Co-N bonding, with no intensity maximum corresponding to Co-Co and Co-O, as shown in Fig. 3f. The XAS results demonstrate the successful and atomically dispersed decoration of Co_{SA}-PMOF by binding the Co atoms to N atoms in the porphyrin rings of the PMOF, consistent with the aberration-corrected HAADF-STEM observations. The atomically decorated Co(II) in PMOF would provide single-electron redox capacity and allow the realization

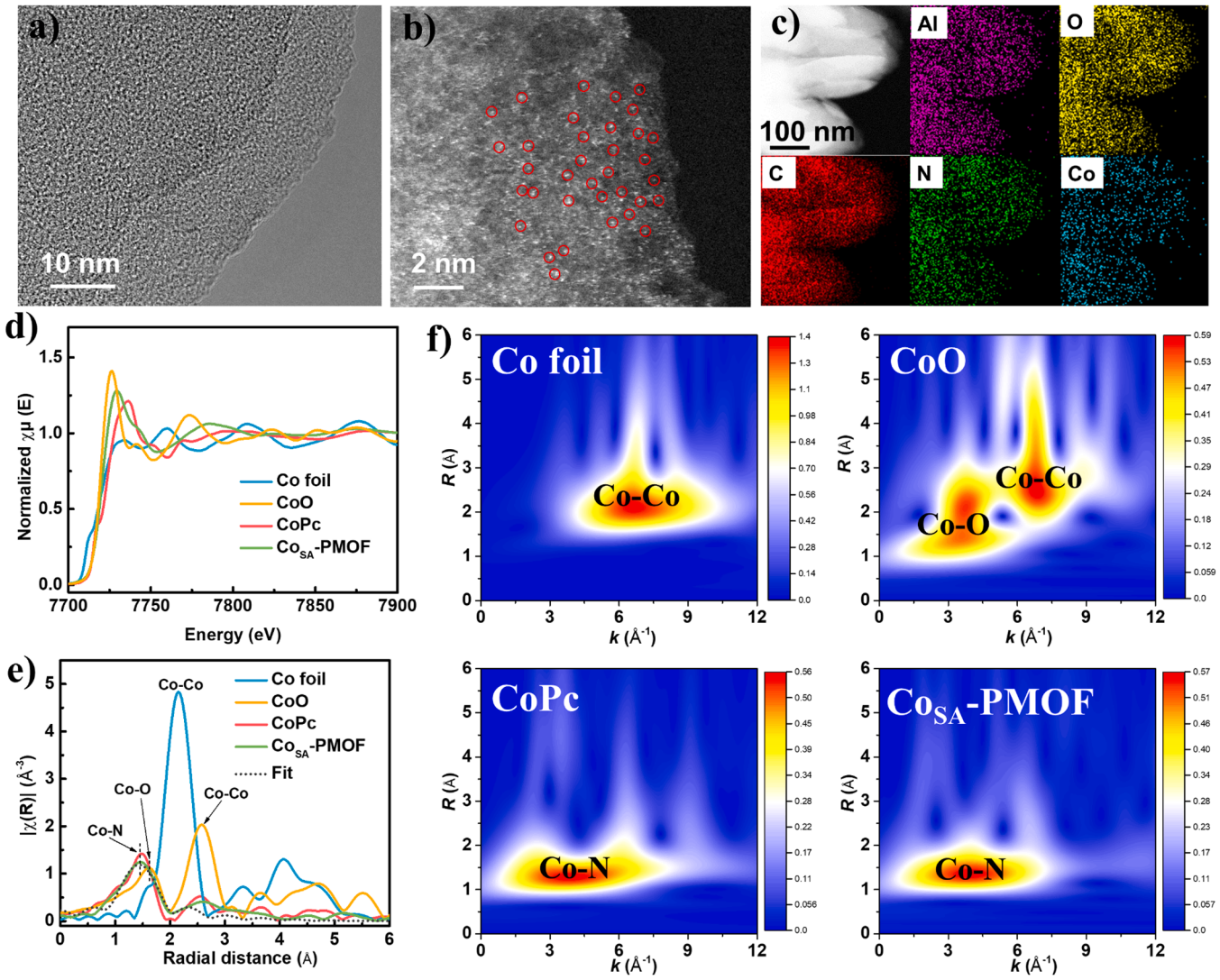

Fig. 3. Structural analysis of Co_{SA}-PMOF: (a) TEM, (b) spherical aberration-corrected HAADF-STEM, and (c) corresponding EDX elemental mapping images of Co_{SA}-PMOF; (d) Co K-edge XANES spectra, (e) Fourier-transformed EXAFS signals, and (f) Co K-edge EXAFS WTs of Co_{SA}-PMOF and standard references.

of Co(II)/Co(III) redox cycling in the porphyrin rings during catalytic reactions with PMS [46].

3.3. Catalytic performance and identification of reactive species

The antibiotic MOX was selected as a model emerging organic pollutant for an experimental study of catalytic organic degradation owing to its ubiquitous pollution and persistent toxicity to ecosystems. The experimental tests on MOX (10 μM) degradation were conducted with 0.5 mM PMS at neutral pH, with 0.1 g L^{-1} catalyst if added. As shown in Fig. 4a, the MOX degradation efficiency was less than 5 % after 6 min when PMS was added alone, indicating a negligible contribution of direct oxidation by PMS without the catalysts. When PMS was added together with the PMOF catalyst, the MOX degradation efficiency was only 22 % after 6 min. In contrast, when Co_{SA}-PMOF was added as the catalyst with PMS, the MOX degradation efficiency was nearly 100 % within 6 min. The results indicate a substantial improvement of the catalytic capability of Co_{SA}-PMOF after decoration of the PMOF with atomically dispersed Co-N_4 sites. The contribution of adsorption by Co_{SA}-PMOF to the MOX removal was only about 8 % (Fig. S2). The catalytic activity was further indicated by the degradation rate constant (k) (Fig. 4b). The k value of MOX degradation in the PMS/Co_{SA}-PMOF system was as high as 0.91 min^{-1}, which is more than 20 times higher than that of the reaction catalyzed by the pristine PMOF (0.04 min^{-1}) and 116 times higher than that catalyzed by the conventional metal oxide catalyst Co_3O_4 (0.008 min^{-1}). The excellent catalytic performance of Co_{SA}-PMOF for MOX degradation is attributable to the high efficiency of the atomically dispersed Co-N_4 sites in the 2D nanosheets for PMS activation. According to the PMS decomposition test, the Co_{SA}-PMOF system demonstrated a significantly faster PMS decomposition rate than that in the PMOF system (Fig. S3), which further proved that the atomically dispersed Co-N_4 sites greatly promoted the activation of PMS. Moreover, the atomic insertion of the CoN_4 active sites endowed Co_{SA}-PMOF with an excellent catalytic capacity, with a turnover frequency (TOF) value of 9.10 min^{-1} for PMS-based AOPs, superior to other current heterogeneous catalysts including MOF, metal oxides, and carbon materials, as well as reported single-atom Co catalysts (Table S3, Supporting Information) [38]. In addition, the Co_{SA}-PMOF catalyst still achieved a MOX degradation efficiency of more than 90 % when dosing a relatively low concentration of PMS (0.1 mM) (Fig. 4c), which can improve its cost-effectiveness in practical applications.

To identify the active radicals generated via catalysis, quenching experiments were conducted using *tert*-butanol (TBA) as the scavenger for •OH and methanol as the scavenger for both •OH and $SO_4^{\bullet-}$ [13,47]. As shown in Fig. 4d, the MOX degradation efficiency decreased only slightly (from 100 % to 93.3 %) when TBA (0.5 M) was added to the

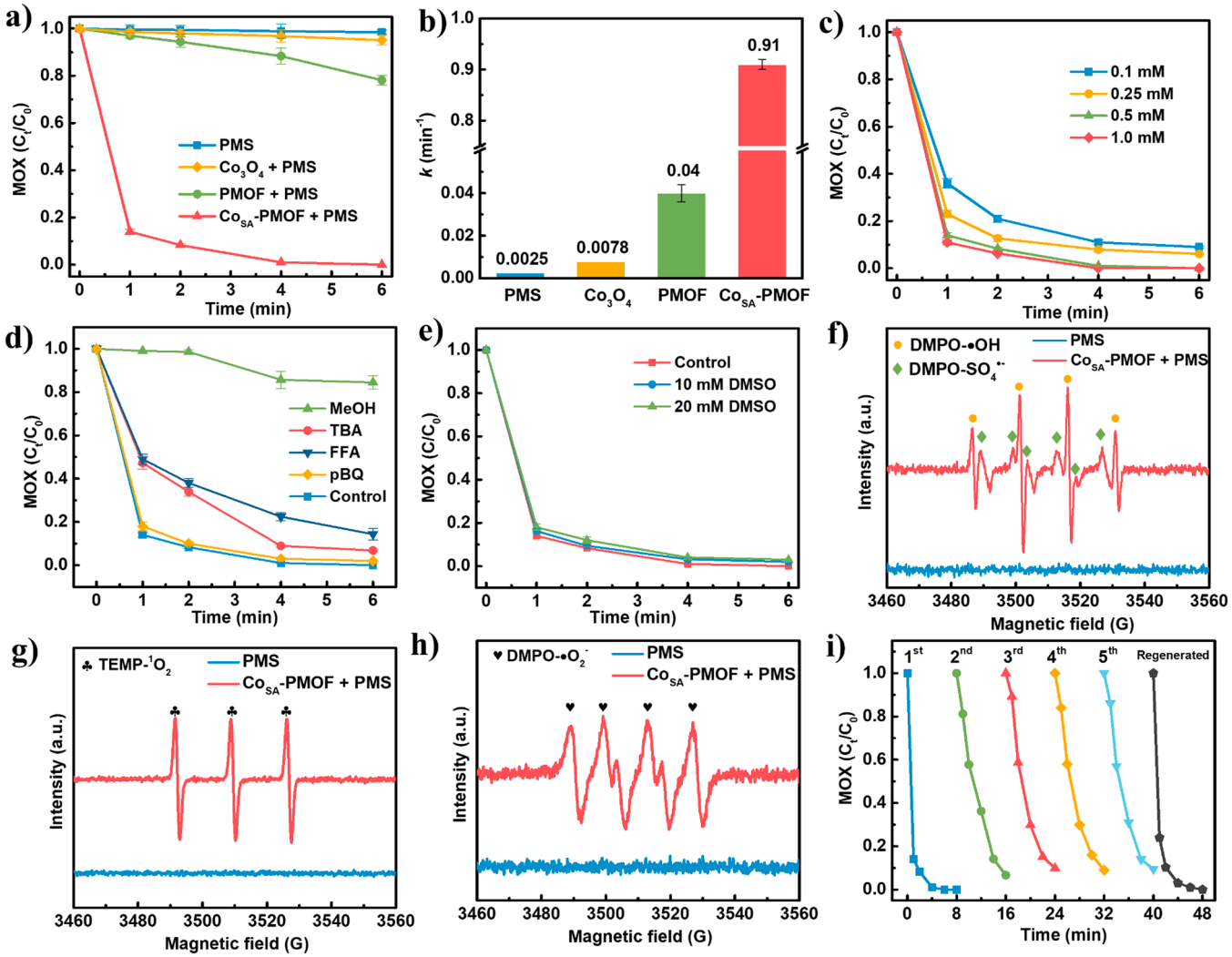

Fig. 4. Experimental tests of catalytic activity: (a) degradation of 10 μM MOX by 0.5 mM PMS with 0.1 g L^{-1} catalyst at neutral pH of 6.8; (b) the MOX degradation rate constants for the different catalysts; (c) comparison of catalytic MOX degradation by Co_{SA}-PMOF at different PMS dosing concentrations; (d) effects of the additions of methanol (0.5 M), TBA (0.5 M), FFA (0.02 M), and pBQ (0.02 M) as the quenching agents on MOX degradation; (e) effect of DMSO on the MOX degradation in the PMS/Co_{SA}-PMOF system; EPR spectra of PMS only and the PMS/Co_{SA}-PMOF system, (f) using DMPO as the spin trap, (g) using TEMP as the spin trap, (h) using DMPO/DMSO as the spin trap; and (f) cycling performance of Co_{SA}-PMOF for MOX degradation.

PMS/Co_{SA}-PMOF system, suggesting a small contribution of •OH to MOX degradation. In contrast, the MOX degradation efficiency significantly decreased from 100 % to 15.6 % when methanol (0.5 M) was added to the system. Comparison of these results indicates that in-situ generated $SO_4^{\bullet-}$ was the dominant active radical contributing to MOX degradation in solution, which is consistent with the report of using $CoFe_2O_4$ as a catalyst to activate PMS for MOX degradation [48]. Additionally, p-benzoquinone (pBQ) was used as the scavenger of $\bullet O_2^-$ in the quenching tests. The slight inhibition of MOX degradation in the presence of pBQ (0.02 M) suggested the minor role of $\bullet O_2^-$ in MOX removal. Considering the possibility that non-radical $^1O_2$ is involved in PMS activation, especially in carbonaceous nanomaterials, furfuryl alcohol (FFA) was used as the scavenger for $^1O_2$ [22,24]. The MOX degradation efficiency decreased by 14.3 % when FFA (0.02 M) was added, indicating the considerable contribution of $^1O_2$ to the observed catalytic MOX degradation. The contributions of the reactive species involved in the reaction system were estimated on the basis of pseudo-first-order kinetics ($Ln(C/C_0) = -kt$) of MOX in the presence of scavengers (Fig. S4) [49]. In the PMS/Co_{SA}-PMOF system, the contributions of $SO_4^{\bullet-}$, •OH, and $^1O_2$ to MOX degradation were around 62 %, 32 %, and 6 %, respectively. The possible generation of high-valent Co−oxo in the PMS/Co_{SA}-PMOF system was investigated by using DMSO as the quenching agent [50]. The MOX degradation efficiency had a minor decrease in the presence of 10 mM and 20 mM DMSO (Fig. 4e), indicating a negligible role of high-valent Co−oxo species in the PMS/Co_{SA}-PMOF system. The results of these quenching experiments indicate that PMS was probably activated by Co_{SA}-PMOF through the radical ($SO_4^{\bullet-}$) generation pathway, leading to effective MOX degradation.

Electronic paramagnetic resonance (EPR) with 5,5-dimethyl-1-pyrroline N-oxide (DMPO) as a spin trap was applied to further confirm the generation of active radicals during PMS activation [51]. As shown in Fig. 4f, no signals were observed when only PMS was added to the test system. With the addition of Co_{SA}-PMOF, the characteristic signals of •DMPO−SO_4^- and •DMPO−OH were both observed, indicating the generation of •OH and $SO_4^{\bullet-}$ in the PMS/ Co_{SA}-PMOF system. The $SO_4^{\bullet-}$ radical was generated in situ during PMS reduction by the single-atom Co(II) sites of Co_{SA}-PMOF (Equation 1). The formation of •OH can be attributed to the reaction between $SO_4^{\bullet-}$ and H_2O (Equation 2) [52]. The EPR test using TEMP as a trapping agent for $^1O_2$ was conducted. The characteristic triplet signals (intensity ratio of 1:1:1 in Fig. 4g) corresponding to TEMP-$^1O_2$ were detected that indicate the existence of $^1O_2$ in the reaction system, which agrees with the quenching experiment

results. The detection of $\bullet O_2^-$ radicals was conducted by using DMPO/DMSO as the trapping agent. The characteristic peak signals (intensity ratio of 1:1:1:1) corresponding to DMPO-$\bullet O_2^-$ were observed (Fig. 4h), indicating the presence of $\bullet O_2^-$ in the reaction system. By combining the EPR results with the quenching experimental results, we can conclude that Co_{SA}-PMOF cleaves PMS to generate reactive $SO_4^{\bullet -}$ radicals for the oxidation and degradation of MOX.

$$Co(II) + HSO_5^- \rightarrow Co(III) + SO_4^{\bullet -} + OH^- \quad (1)$$

$$SO_4^{\bullet -} + H_2O \rightarrow SO_4^{2-} + \cdot OH + H^+ \quad (2)$$

The Co_{SA}-PMOF catalyst maintained its high MOX degradation efficiency (>97 %) in the presence of inorganic anions, including SO_4^{2-}, HCO_3^-, Cl^- and NO_3^- (Fig. S5), in water, demonstrating its low sensitivity to competing ions and high applicability in a complex wastewater matrix. A cycling test was conducted to evaluate the stability of the single-atom catalyst. Co_{SA}-PMOF exhibited a stable structure and performance in terms of PMS activation and MOX degradation efficiency; after five cycles (8 min per cycle), the degradation efficiency was maintained at 91 % (Fig. 4i), and the structure of the catalyst remained intact as demonstrated by SEM and XRD (Figs. S6 and S7, Supporting Information). The decreased rate constant was possibly attributed to the attachment of the intermediates and products on the active CoN_4 sites. The performance of the used Co_{SA}-PMOF catalysts can be well recovered by washing with ethanol and thermal treatment at 200 °C in N_2 for 6 h. As shown in Fig. 4i, the regenerated Co_{SA}-PMOF catalyst displayed a promising recovery of its catalytic activity. A trace level of leached Co (< 20 μg L^{-1}) was detected during the test (Table S4, Supporting Information), which is far below the limit in reclaimed water (50 μg L^{-1}) set by the U.S. EPA [53].

3.4. Self-assembled 2D-Co_{SA}-PMOF lamellar membrane for catalytic water treatment

Catalyst immobilization is a desirable approach that would enable the practical application of catalytic AOPs for wastewater treatment and reuse. A catalytic lamellar membrane composed of 2D Co_{SA}-PMOF was constructed via self-assembly. As illustrated in Fig. 1, the as-prepared 2D Co_{SA}-PMOF was well dispersed in water by sonication and gently processed via vacuum filtration on a prescribed porous polyvinylidene fluoride (PVDF) substrate. Subsequently, the catalyst self-assembled to form a stable layer on the backing substrate. The obtained layer appeared as a tightly stacked lamellar membrane, which was presumably held together by π–π interactions between adjacent 2D nanosheets. A photograph of the Co_{SA}-PMOF membrane on a PVDF substrate is presented in Fig. 5a, and b shows the morphology of the membrane surface as uniformly assembled 2D nanosheets. The as-prepared Co_{SA}-PMOF membrane had a thickness of 8.1 ± 0.4 μm with a mass loading of 0.3 $mg_{catalyst}$ cm^{-2}. The water contact angle of 35.4° suggests that the membrane is hydrophilic (Fig. S8). The permeability of this catalytic membrane was as high as 135.2 L m^{-2} h^{-1} bar^{-1} (Fig. S9), indicating its potential usage in microfiltration. Unlike a batch system with a suspended catalyst, the immobilized Co_{SA}-PMOF membrane can be readily used in a simple one-step water and wastewater filtration treatment, eliminating the need for redundant post-treatments such as filtration and centrifugation to separate and recover the catalysts. As the PMS activator, the catalytic lamellar membrane is applied to enhance the catalytic efficacy in the flow-through mode by confining the PMS and pollutant molecules to the vicinity of the active sites on the Co_{SA}-PMOF nanosheets within the membrane.

As a catalytic membrane, the lamellar membrane can achieve ultrahigh efficiency in the continuous treatment of organic pollutants in

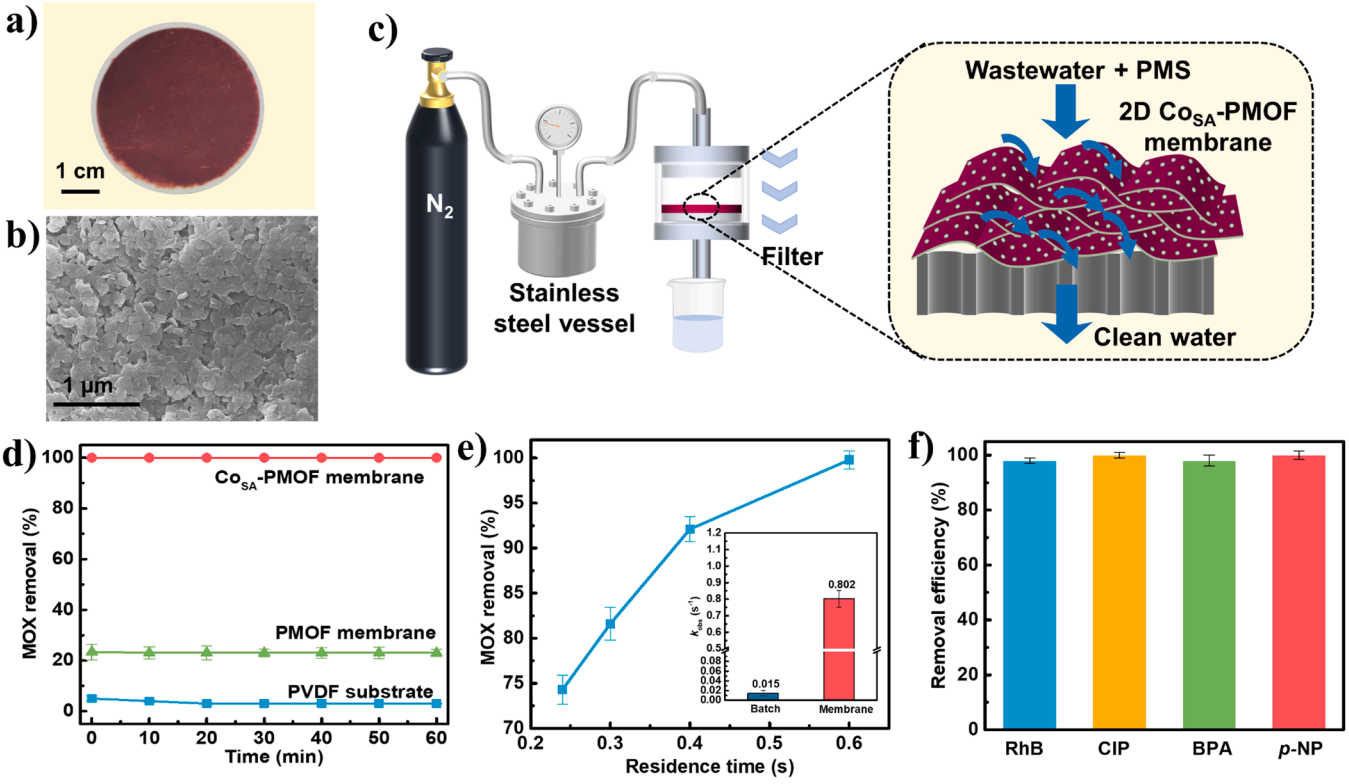

Fig. 5. The structure and catalytic performance of the 2D Co_{SA}-PMOF membrane: (a) photo and (b) SEM image of the Co_{SA}-PMOF membrane; (c) schematic of the lamellar membrane filtration system for wastewater treatment; (d) degradation of 10 μM MOX with 0.5 mM PMS through the PVDF substrate alone or with the PMOF membrane or Co_{SA}-PMOF membrane on the PVDF substrate at a flux of 48 LMH; (e) degradation of 10 μM MOX with 0.5 mM PMS through the Co_{SA}-PMOF membrane at different filtration rates with different residence times (inset: k_{obs} of MOX degradation in the batch reactor and membrane filtration system); and (f) versatility of the Co_{SA}-PMOF membrane for the removal of several persistent organic pollutants, including RhB, CIP, BPA, and *p*-NP.

wastewater. As illustrated in Fig. 5c, the as-prepared Co_{SA}-PMOF membrane was sealed in a flow-through filtration cell during continuous filtration–degradation experiments. The feed water containing MOX and PMS was forced by constant gas pressure to permeate the membrane in a continuous single-pass operation, and the MOX degradation efficiencies of the different filter types are given in Fig. 5d. Only slight MOX removal was observed with the PVDF substrate alone (degradation efficiency~3 %), suggesting that the backing substrate had little interaction with MOX molecules during filtration. Remarkably, the 2D Co_{SA}-PMOF lamellar membrane achieved a 100 % MOX degradation efficiency at a high flux of 48 L m^{-2} h^{-1} (LMH), while the precursor PMOF membrane (without Co atom decoration) had a much lower efficiency of only 23.2 %. The superb oxidation performance of the 2D Co_{SA}-PMOF membrane within a short residence time (< 1 s) is attributed to both the high catalytic activity of the atomically dispersed Co-N_4 sites for PMS activation and the confinement effect that greatly enhanced the contact of PMS and MOX with the catalytic sites within the membrane.

The effect of flux on the treatment performance of the catalytic membrane was also investigated (Fig. S10). Generally, the MOX degradation efficiency decreased as the filtration flux increased due to the reduction in retention time through the reactive membrane, and the relationship between MOX degradation and the residence time inside the membrane was quantified (Figs. 5e and S11). Similar to the reaction time effect in the batch system, a longer residence time through the membrane resulted in a higher MOX degradation efficiency. However, the first-order rate constant, k_{obs}, in the Co_{SA}-PMOF membrane was determined to be 0.802 s^{-1}, which was ~52 times higher than that in the batch reactor with suspended Co_{SA}-PMOF catalysts (0.015 s^{-1}). The rate constant normalized to the mass of the catalyst (k_{nor}) of the Co_{SA}-PMOF membrane (212.8 s^{-1} g^{-1}) was about 57 times that of the suspended powder catalyst (3.75 s^{-1} g^{-1}). The significant improvement was probably due to the confinement effect in the 2D nano-interspace of the Co_{SA}-PMOF lamellar membrane, which would enable the high exposure and accessibility of the active CoN_4 sites for the production of reactive $SO_4^{\bullet-}$ for the oxidation of MOX molecules. Meanwhile, the fluid confined in the interspacing of the membrane may have facilitated material transport to enable rapid reactions between in-situ generated radicals and the target organic pollutants [40].

For comparison with the treatment without the confinement effect, the MOX degradation test with a conventional continuous-flow column reactor filled with Co_{SA}-PMOF powder was conducted. The Co_{SA}-PMOF in the column reactor exhibited a ~63 % removal of MOX in the single-pass treatment (Fig. S14), which is significantly lower than the Co_{SA}-PMOF lamellar membrane (100 %) with the same catalyst load. These results imply the confinement effect in the 2D nanopores of the Co_{SA}-PMOF lamellar membrane on the enhanced MOX degradation. Overall, a MOX degradation efficiency exceeding 92 % was achieved at a filtration flux of as high as 72 L m^{-2} h^{-1}, and the corresponding permeability (135 L m^{-2} h^{-1} bar^{-1}) was much higher than that of a recently reported graphene oxide catalytic membrane (1.2 L m^{-2} h^{-1} bar^{-1}) [41].

3.5. Applicability and stability of the Co_{SA}-PMOF membrane

The 2D Co_{SA}-PMOF lamellar membrane can be readily fabricated on different backing substrates, e.g., an Al_2O_3 ceramic membrane. The performance of a Co_{SA}-PMOF membrane on a ceramic substrate for catalytic MOX degradation was similar to the performance on a PVDF substrate. The as-prepared Co_{SA}-PMOF membrane on the Al_2O_3 substrate yielded 100 % MOX degradation efficiency at a flux of 48 LMH, compared with only 5.2 % for the pristine Al_2O_3 ceramic substrate (Fig. S12). We also demonstrated the feasibility and versatility of the Co_{SA}-PMOF membrane for the removal of a range of persistent organic pollutants of recent concern, including rhodamine B (RhB), an azo dye widely used in the textile industry; ciprofloxacin (CIP), a widely used antibiotic; bisphenol A (BPA), a typical endocrine-disrupting chemical (EDCs) found in surface water and groundwater; and *p*-nitrophenol (*p*-NP), a highly toxic and persistent chemical used extensively in the pharmaceutical and pesticide chemical industries [54,55]. As shown in Fig. 5f, all of these representative emerging organic pollutants were rapidly degraded (efficiency > 98 %) by PMS through the reactive Co_{SA}-PMOF membrane.

The MOX removal performance of the Co_{SA}-PMOF lamellar membrane in different pH and water matrix conditions was further investigated. As shown in Fig. 6a, the 2D Co_{SA}-PMOF lamellar membrane maintained its nearly 100 % MOX degradation efficiency as the solution pH increased from 3 to 9. When further increasing the pH to 11, the MOX removal decreased to about 73 %. Overall, the PMS/Co_{SA}-PMOF lamellar membrane system performed well in a broad pH range (3−9). The feasibility of Co_{SA}-PMOF in different water matrices was also studied by adding MOX (10 μM) to tap water, river water, and the treated secondary wastewater effluent (Fig. 6b). The Co_{SA}-PMOF lamellar membrane achieved >99 % MOX removal in tap water, river water, and the secondary effluent, indicating its applicability in actual water and wastewater treatment.

The effect of natural organic matter (NOM) on the MOX removal in the PMS/Co_{SA}-PMOF membrane system was investigated by adding human acid (HA, 10 mg L^{-1}) to the solution. As shown in Fig. 6c, when HA was added, the MOX removal by the Co_{SA}-PMOF membrane with 0.5 mM PMS decreased from 100 % to 88.2 %. The reduced MOX degradation efficiency was probably caused by the consumption of reactive radicals by the electron-rich groups in HA ($k_{SO4\bullet-/NOM} = 10^8$ M^{-1} s^{-1}) [56]. However, when PMS was dosed at a higher concentration of 2 mM, HA in water showed a negligible effect (<2 %) on the MOX removal, which is likely due to the degradation of HA by the sufficient amount of $SO_4^{\bullet-}$ radicals generated. These results also imply that the Co_{SA}-PMOF lamellar membrane with a sufficient PMS dosing can remove both emerging pollutants and natural organic matter from water and wastewater.

The membrane fouling was investigated by monitoring the permeability of the membrane in the presence of 10 mg L^{-1} HA for a long operation period (10 h). As shown in Fig. 6d, without the dosing of PMS, the permeability of the Co_{SA}-PMOF lamellar membrane dropped from 135.8 to 88.6 LMH bar^{-1} after 10 h. In contrast, when 2 mM PMS was dosed into the influent, the permeability of the Co_{SA}-PMOF lamellar membrane decreased only slightly by ~7 % after 10 h. The fouling comparison indicates that the PMS/Co_{SA}-PMOF membrane can alleviate the membrane fouling problem via catalytic destruction of organic foulants. In addition, the contact angle of the used membrane (36.2°) was close to that of the fresh Co_{SA}-PMOF membrane (35.4°), suggesting that the hydrophobic HA on the membrane was effectively degraded by the PMS-based oxidation.

The Co_{SA}-PMOF lamellar membrane also exhibited high stability and maintained its physical structure and chemical properties after a long period of operation. Specifically, after 3 days of filtration, the Co_{SA}-PMOF membrane exhibited a lack of swelling (intact surface; Fig. S13), nearly unchanged hydrophilicity (similar contact angles of around 35.6° over time; Fig. S14), and preserved high catalytic performance (Fig. S15). The excellent stability of the Co_{SA}-PMOF lamellar membrane can be attributed to strong bonding of the adjacent 2D nanosheets via attractive π–π interactions between parallel porphyrin ligands [57]. Another concern surrounding the use of catalytic AOPs for wastewater treatment is the potential leaching of metal ions from the catalysts. We showed experimentally that the concentration of leached Co ions in the permeate was below 12 μg L^{-1} (Fig. S16), which is much lower than the U.S. EPA reclaimed water limit of 50 μg L^{-1}. The high stability of Co in the Co_{SA}-PMOF lamellar membrane is presumably due to the highly stable π-conjugated macrocyclic metalloporphyrin structure (CoN_4 in porphyrin rings). Overall, the novel catalytic Co_{SA}-PMOF membrane developed in this research possesses superior advantages as a radical activator in water pollution control applications, including the rapid removal of a wide range of organic pollutants at a very high filtration flux, a simple system, easy operation, high stability for long-term usage,

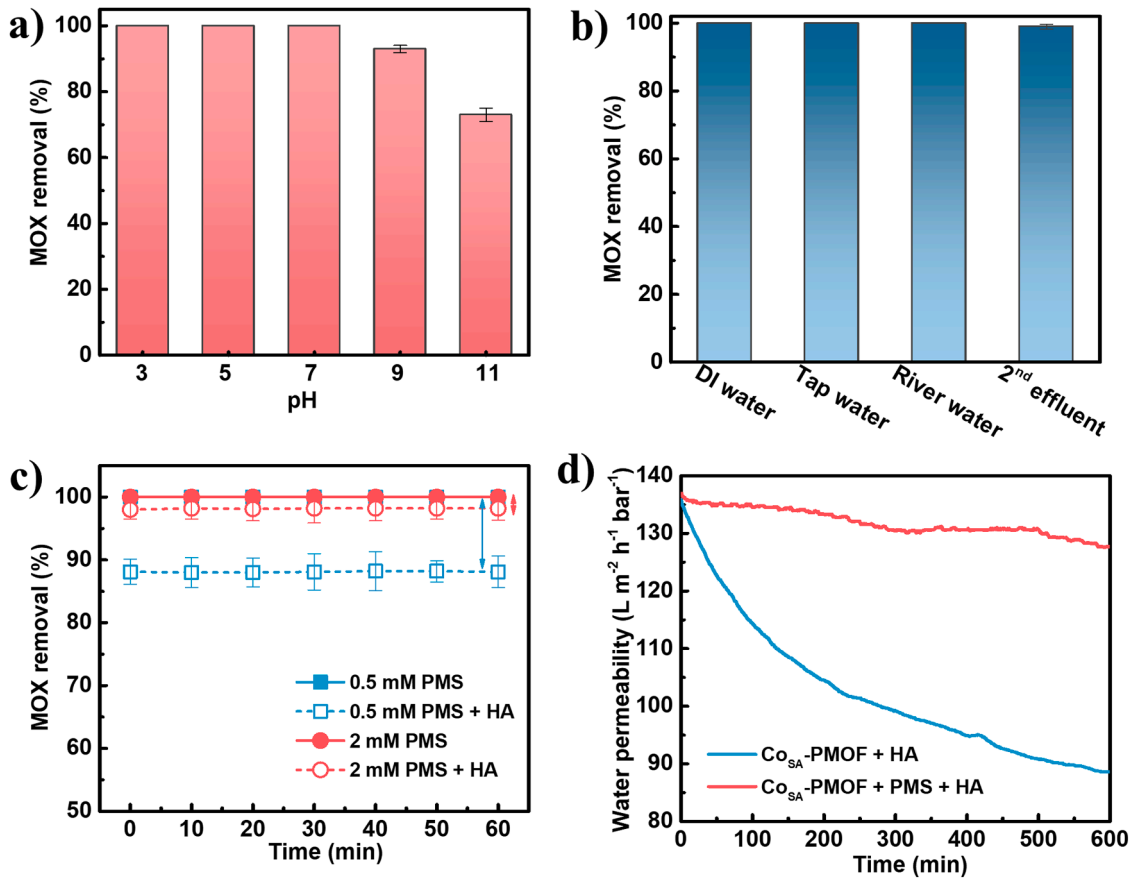

Fig. 6. The MOX degradation performance of the Co_{SA}-PMOF lamellar membrane: (a) at different pH levels, (b) in different water matrices, (c) with and without the addition of 10 mg L^{-1} HA; and (d) the filtration performance of the Co_{SA}-PMOF lamellar membrane in the different water matrices.

and negligible metal leaching potential.

3.6. Catalytic mechanism

The catalytic mechanism of Co_{SA}-PMOF was investigated through density functional theory (DFT) calculations and experiments. Fig. 7a shows a color-filled valence charge density map of an atomically dispersed CoN_4 site in Co_{SA}-PMOF after configuration. As determined by XPS and XAS analyses, the positive Co in the center of the porphyrin ring is surrounded by N, which facilitates the adsorption of the negative O in PMS. The EPR results confirmed the electron properties of Co_{SA}-PMOF (Fig. 7b). The observed high signal intensity suggests a high abundance of unpaired electrons of Co atoms in the porphyrin rings of Co_{SA}-PMOF, enabling electron transfer for the redox reaction of PMS activation. The electrons eventually come from PMS or organic pollutants during the Co-facilitated catalytic reaction cycle. Electron transfer was further evidenced by an electrochemical characterization test, i.e., linear sweep voltammetry (LSV) analysis. The current of the Co_{SA}-PMOF electrode decreased when PMS was added to the solution (Fig. 7c), signifying electron transfer from Co to PMS in the system. When adding MOX to the solution, the current was further decreased, which suggests the possible involvement of the activated PMS*-mediated electron transfer mechanism. The activated PMS on the catalyst surface was likely to abstract electrons from MOX molecules, leading to its oxidation and degradation. The open-circuit potential (OCP) of the working electrode with the Co_{SA}-PMOF catalyst displayed a significant jump after adding PMS in the solution (Fig. 7d), suggesting the formation of reactive PMS complexes on the surface of Co_{SA}-PMOF. In contrast, the OCP of the working electrode of PMOF showed a weak response after the PMS addition. The electrochemical impedance spectroscopy (EIS) results also indicated that the electron-transfer resistance (R_{ct}) of Co_{SA}-PMOF was much smaller, only about 4 % that of PMOF (Fig. S17). Thus, the single atomic Co sites endow the Co_{SA}-PMOF catalyst with a greatly enhanced electron-transfer capability for PMS activation.

DFT calculations further revealed the mechanism and related pathways of PMS activation by the decorated single-atom Co sites centered in the porphyrin rings of Co_{SA}-PMOF. Fig. 8a and b show the possible configurations of PMS towards the Co site, which have adsorption energies (E_{ads}) of − 3.06 and − 3.20 eV, respectively. That is, the adsorption of O in O-O (in Fig. 8b) is more favorable in terms of adsorption energy. The O-O bond length (l_{O-O}) in free PMS was 1.35 Å but stretched to 1.48 Å after PMS was adsorbed on Co_{SA}-PMOF, facilitating the O-O bond activation and $SO_4^{\bullet-}$ production [58]. Thus, PMS activation by Co_{SA}-PMOF was likely to have involved a radical pathway for the generation of $SO_4^{\bullet-}$, which possesses a strong oxidation capacity for organic degradation. These DFT calculations are also consistent with the results of our above-described quenching experiments that identified $SO_4^{\bullet-}$ as the dominant oxidation species in MOX degradation. Fig. 8c illustrates the difference in electron density between PMS and Co_{SA}-P-MOF. Electron transfer from Co to PMS results from the chemisorption of PMS on Co(II) sites, suggesting that each single Co atom in Co_{SA}-PMOF served as an active electron donor to PMS, in accordance with the LSV results. Bader charge analysis of Co in Co_{SA}-PMOF before and after the PMS adsorption further confirmed the electron transfer (0.26 e) from Co to PMS. Therefore, during PMS activation, the Co atom in the porphyrin ring of Co_{SA}-PMOF functions as the active site for PMS adsorption and reduction, leading to cleavage of the O-O bond and the generation of reactive $SO_4^{\bullet-}$ radicals.

Drawing on the results of the above-described comprehensive studies, a reaction mechanism can be revealed for PMS activation by

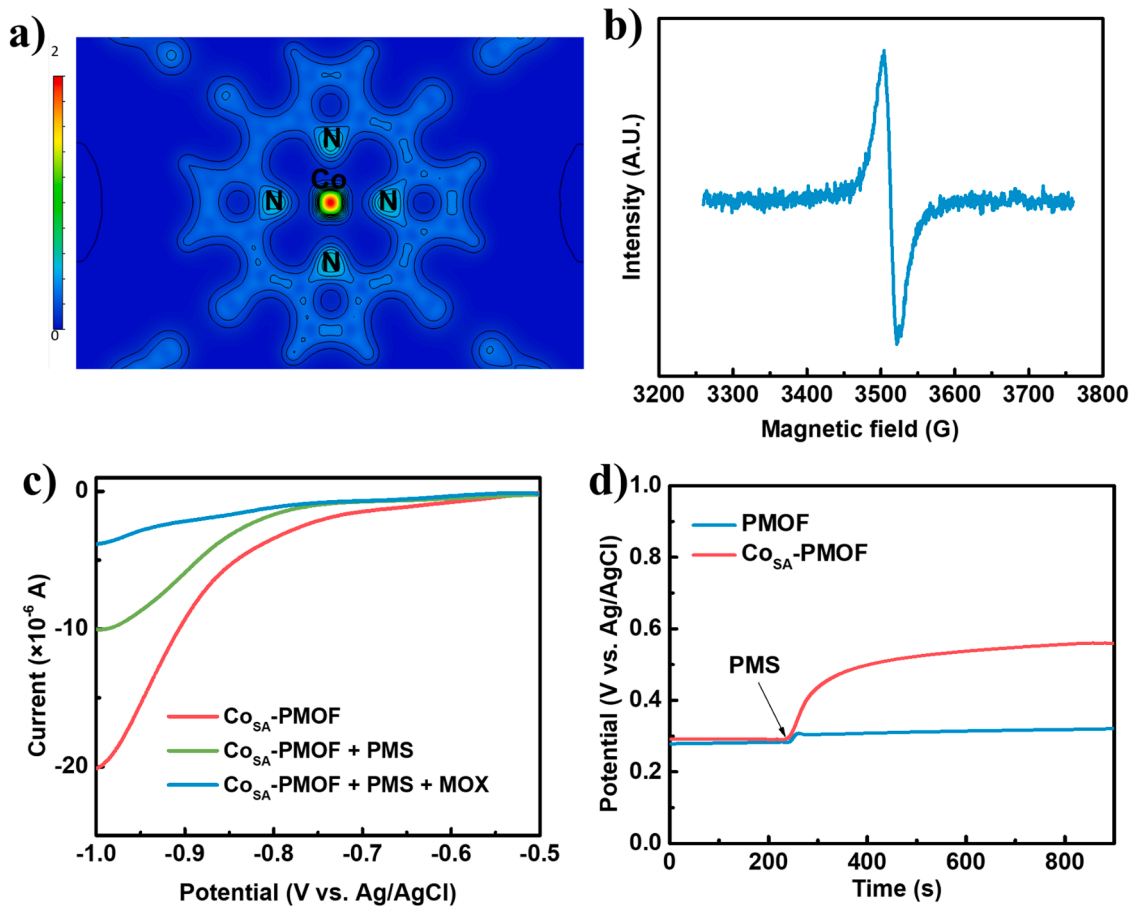

Fig. 7. (a) 2D color-filled valence charge density map of Co_{SA}-PMOF; (b) EPR spectrum of Co_{SA}-PMOF at room temperature; (c) LSV curves of Co_{SA}-PMOF in different test solutions; and (d) the open-circuit potentials of the PMOF and Co_{SA}-PMOF working electrodes before and after the PMS addition.

Co_{SA}-PMOF (Fig. 8d). PMS is easily accessible to the atomically dispersed Co(II) sites in the 2D lamellar Co_{SA}-PMOF membrane. The Co (II) sites act as electron donors for PMS reduction during PMS adsorption and activation. As a result of electron transfer from Co to PMS, the O-O bond in PMS is cleaved and reactive $SO_4^{\bullet-}$ is generated for organic degradation. After the release of $SO_4^{\bullet-}$, the Co(II) sites are changed to Co (III) within the porphyrin rings and can be readily reduced to Co(II) by $SO_5^{\bullet-}$ [59]. Co(II)/Co(III) redox cycling during PMS activation was further verified by XPS analysis of Co_{SA}-PMOF after use. The results confirmed the co-existence of both Co(II) and Co(III) in the used catalyst (Fig. S18). Co(II)/Co(III) redox within the porphyrin rings endows Co_{SA}-PMOF with both an ultra-high efficiency for organic pollutant degradation and a highly stable cycling performance in catalytic reactions. In addition, according to our analysis of intermediates identified by UPLC-QTOF-MS (Fig. S19 and Table S5), three possible main pathways of catalytic MOX oxidation by PMS/Co_{SA}-PMOF are proposed, namely decarboxylation, defluorination, and heterocycle cleavage (Fig. S20) [55,60,61], which lead to MOX degradation and detoxication. The total organic carbon (TOC) removal efficiency was about 35 %, indicating considerable mineralization of MOX into CO_2 and H_2O by catalytic PMS oxidation.

4. Conclusions

In summary, a water-stable lamellar membrane composed of a 2D MOF with atomically dispersed CoN_4 sites was developed as an efficient catalytic filter for PMS activation and wastewater treatment. The single Co atoms serving as the active sites in Co_{SA}-PMOF favor PMS adsorption and reduction to generate reactive $SO_4^{\bullet-}$. The lamellar membrane assembled from 2D Co_{SA}-PMOF nanosheets not only achieves effective immobilization of the catalyst but also confines the reactants in the vicinity of the active sites to boost the organic degradation efficiency, which was 100 % for MOX at a high filtration flux of 48 LMH. This result places the Co_{SA}-PMOF membrane among the state-of-the-art catalytic membranes in AOP for water and wastewater treatment. By combining quenching tests, EPR, electrochemical analysis, and DFT calculations, the catalytic mechanism of this Fenton-like process was revealed: the Co-decorated porphyrin rings of the catalyst contain abundant unpaired electrons for PMS activation. In particular, the atomically dispersed CoN_4 in Co_{SA}-PMOF acts as an active site for PMS adsorption and reduction, and reactive $SO_4^{\bullet-}$ resulting from O-O bond cleavage serves as the primary free radical for organic degradation. Co(II)/Co(III) redox in the center of each decorated porphyrin ring endows Co_{SA}-PMOF with high stability and excellent cycle performance. The research findings provide essential insights into the design and preparation of new catalytic lamellar membranes via atomic decoration of active sites in 2D MOFs for high-rate and high-performance wastewater treatment and reuse applications.

CRediT authorship contribution statement

Chao Yang: Conceptualization, Investigation, Methodology, Formal analysis, Writing – original draft. **Shanshan Shang:** Conceptualization, Formal analysis. **Yiang Fan:** Formal analysis, Visualization. **Kaimin Shih:** Methodology, Software. **Xiao-yan Li**: Supervision, Methodology, Writing – review & editing, Funding acquisition. **Lin Lin**:Formal analysis, Writing – review & editing.

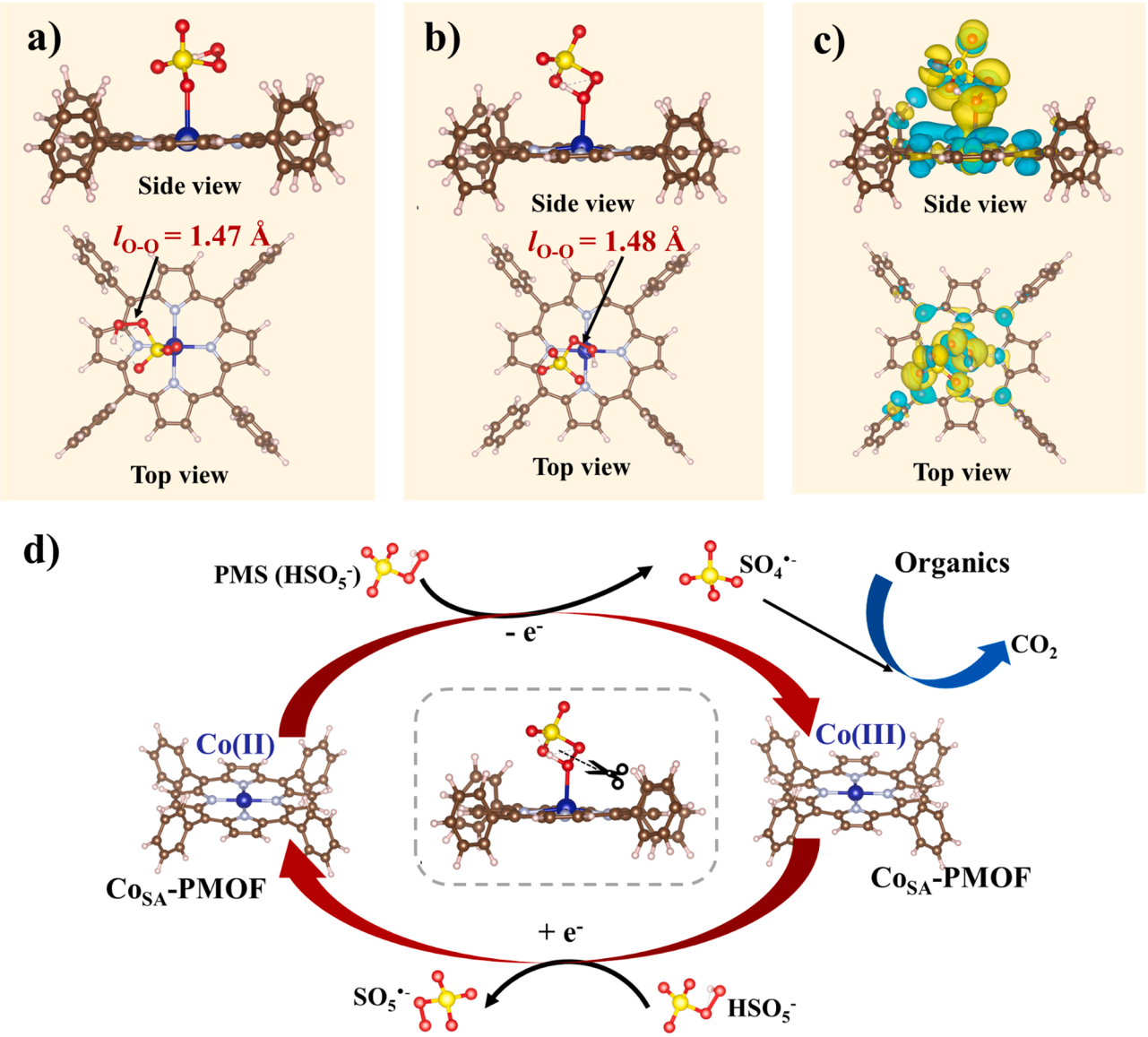

Fig. 8. DFT analyses of the catalytic mechanism of Co_{SA}-PMOF: (a) and (b) PMS adsorption on the atomically inserted Co(II) sites of Co_{SA}-PMOF; (c) difference in electron density between PMS and Co_{SA}-PMOF; and (d) proposed reaction paths for PMS activation by Co_{SA}-PMOF.

Declaration of Competing Interest

The authors declare that they have no known competing financial interests or personal relationships that could have appeared to influence the work reported in this paper.

Data Availability

No data was used for the research described in the article.

Acknowledgments

This research was financially supported by the National Natural Science Foundation of China (Projects 51978369 and 51908316), the Basic and Applied Basic Research Foundation (Project 2020A1515111205) of the GuangDong Government, the Municipal Science and Technology Innovation Commission (Projects JCYJ20190809172805540, WDZC20200818162958002, and RCBS20200714114942215) of the Shenzhen Government, the Research Grants Council (Projects 17210219 and T21-711/16R) and the Innovation and Technology Fund (Project ITS/242/20FP) of the Hong Kong Government, China.

Appendix A. Supporting information

Supplementary data associated with this article can be found in the online version at doi:10.1016/j.apcatb.2022.122344.

References

[1] L.A. Schaider, K.M. Rodgers, R.A. Rudel, Review of organic wastewater compound concentrations and removal in onsite wastewater treatment systems, Environ. Sci. Technol. 51 (2017) 7304–7317.
[2] L. Akhtar, M. Ahmad, S. Iqbal, A.A. Abdelhafez, M.T. Mehran, Biochars' adsorption performance towards moxifloxacin and ofloxacin in aqueous solution: Role of pyrolysis temperature and biomass type, Environ. Technol. Innov. 24 (2021), 101912.
[3] N. Nasrollahi, V. Vatanpour, A. Khataee, Removal of antibiotics from wastewaters by membrane technology: limitations, successes, and future improvements, Sci. Total. Environ. 838 (2022), 156010.
[4] C. Yang, S. Shang, X.Y. Li, Oxygen-vacancy-enriched substrate-less SnOx/La-Sb anode for high-performance electrocatalytic oxidation of antibiotics in wastewater, J. Hazard. Mater. 436 (2022), 129212.

[5] B.C. Hodges, E.L. Cates, J.H. Kim, Challenges and prospects of advanced oxidation water treatment processes using catalytic nanomaterials, Nat. Nanotechnol. 13 (2018) 642–650.

[6] S. Mei, G. Huang, X. Rui, L. Li, Mi Ke, X. Pan, Z. Wang, X. Yang, H. Yu, Y. Yu, Sequential assembly tailored interior of porous carbon spheres for boosted water decontamination through peroxymonosulfate activation, Adv. Funct. Mater. 32 (2022), 2111184.

[7] G.P. Anipsitakis, D.D. Dionysiou, Degradation of organic contaminants in water with sulfate radicals generated by the conjunction of peroxymonosulfate with cobalt, Environ. Sci. Technol. 37 (2003) 4790–4797.

[8] Y.H. Guan, J. Ma, X.C. Li, J.Y. Fang, L.W. Chen, Influence of pH on the formation of sulfate and hydroxyl radicals in the UV/peroxymonosulfate system, Environ. Sci. Technol. 45 (2011) 9308–9314.

[9] G.P. Anipsitakis, D.D. Dionysiou, Radical generation by the interaction of transition metals with common oxidants, Environ. Sci. Technol. 38 (2004) 3705–3712.

[10] M. Feng, Z. Wang, D.D. Dionysiou, V.K. Sharma, Metal-mediated oxidation of fluoroquinolone antibiotics in water: a review on kinetics, transformation products, and toxicity assessment, J. Hazard. Mater. 344 (2018) 1136–1154.

[11] W. Li, X. He, B. Li, B. Zhang, T. Liu, Y. Hu, J. Ma, Structural tuning of multishelled hollow microspheres for boosted peroxymonosulfate activation and selectivity: Role of surface superoxide radical, Appl. Catal. B: Environ. 305 (2022), 121019.

[12] F. Chen, L.L. Liu, J.J. Chen, W.W. Li, Y.P. Chen, Y.J. Zhang, J.H. Wu, S.C. Mei, Q. Yang, H.Q. Yu, Efficient decontamination of organic pollutants under high salinity conditions by a nonradical peroxymonosulfate activation system, Water Res. 191 (2021), 116799.

[13] X. Li, X. Huang, S. Xi, S. Miao, J. Ding, W. Cai, S. Liu, X. Yang, H. Yang, J. Gao, J. Wang, Y. Huang, T. Zhang, B. Liu, Single cobalt atoms anchored on porous N-doped graphene with dual reaction sites for efficient Fenton-like catalysis, J. Am. Chem. Soc. 140 (2018) 12469–12475.

[14] J. Ali, L. Wenli, A. Shahzad, J. Ifthikar, G.G. Aregay, Z. Shahib II, Z. Elkhlifi, Z. Chen, Regulating the redox centers of Fe through the enrichment of Mo moiety for persulfate activation: A new strategy to achieve maximum persulfate utilization efficiency, Water Res. 181 (2020), 115862.

[15] J. Zhu, J. Wang, C. Shan, J. Zhang, L. Lv, B. Pan, Durable activation of peroxymonosulfate mediated by Co-doped mesoporous $FePO_4$ via charge redistribution for atrazine degradation, Chem. Eng. J. 375 (2019), 122009.

[16] Y. Fan, Z. Zhou, Y. Feng, Y. Zhou, L. Wen, K. Shih, Degradation mechanisms of ofloxacin and cefazolin using peroxymonosulfate activated by reduced graphene oxide-$CoFe_2O_4$ composites, Chem. Eng. J. 383 (2020), 123056.

[17] P.R. Shukla, S. Wang, H. Sun, H.M. Ang, M. Tadé, Activated carbon supported cobalt catalysts for advanced oxidation of organic contaminants in aqueous solution, Appl. Catal. B: Environ. 100 (2010) 529–534.

[18] P. Hu, M. Long, Cobalt-catalyzed sulfate radical-based advanced oxidation: a review on heterogeneous catalysts and applications, Appl. Catal. B: Environ. 181 (2016) 103–117.

[19] X. Duan, H. Sun, Y. Wang, J. Kang, S. Wang, N-doping-induced nonradical reaction on single-walled carbon nanotubes for catalytic phenol oxidation, ACS Catal. 5 (2014) 553–559.

[20] Y. Feng, P.H. Lee, D. Wu, K. Shih, Surface-bound sulfate radical-dominated degradation of 1,4-dioxane by alumina-supported palladium (Pd/Al_2O_3) catalyzed peroxymonosulfate, Water Res. 120 (2017) 12–21.

[21] P. Cai, J. Zhao, X. Zhang, T. Zhang, G. Yin, S. Chen, C. Dong, Y. Huang, Y. Sun, D. Yang, B. Xing, Synergy between cobalt and nickel on $NiCo_2O_4$ nanosheets promotes peroxymonosulfate activation for efficient norfloxacin degradation, Appl. Catal. B: Environ. 306 (2022), 121091.

[22] X. Mi, P. Wang, S. Xu, L. Su, H. Zhong, H. Wang, Y. Li, S. Zhan, Almost 100% peroxymonosulfate conversion to singlet oxygen on single-atom CoN_{2+2} sites, Angew. Chem. Int. Ed. 60 (2021) 4588–4593.

[23] X. Li, J. Wang, X. Duan, Y. Li, X. Fan, G. Zhang, F. Zhang, W. Peng, Fine-tuning radical/nonradical pathways on graphene by porous engineering and doping strategies, ACS Catal. 11 (2021) 4848–4861.

[24] Y. Zou, J. Hu, B. Li, L. Lin, Y. Li, F. Liu, X.Y. Li, Tailoring the coordination environment of cobalt in a single-atom catalyst through phosphorus doping for enhanced activation of peroxymonosulfate and thus efficient degradation of sulfadiazine, Appl. Catal. B: Environ. 312 (2022), 121408.

[25] M. Moses-DeBusk, M. Yoon, L.F. Allard, D.R. Mullins, Z. Wu, X. Yang, G. Veith, G. M. Stocks, C.K. Narula, CO oxidation on supported single Pt atoms: experimental and ab initio density functional studies of CO interaction with Pt atom on theta-Al_2O_3(010) surface, J. Am. Chem. Soc. 135 (2013) 12634–12645.

[26] Z. Zhang, Y. Zhu, H. Asakura, B. Zhang, J. Zhang, M. Zhou, Y. Han, T. Tanaka, A. Wang, T. Zhang, N. Yan, Thermally stable single atom Pt/m-Al_2O_3 for selective hydrogenation and CO oxidation, Nat. Commun. 8 (2017) 16100.

[27] H.C. Zhou, J.R. Long, O.M. Yaghi, Introduction to metal-organic frameworks, Chem. Rev. 112 (2012) 673–674.

[28] S. Shang, W. Xiong, C. Yang, B. Johannessen, R. Liu, H.Y. Hsu, Q. Gu, M.K. H. Leung, J. Shang, Atomically dispersed iron metal site in a porphyrin-based metal-organic framework for photocatalytic nitrogen fixation, ACS Nano 15 (2021) 9670–9678.

[29] S. Lu, L. Liu, H. Demissie, G. An, D. Wang, Design and application of metal-organic frameworks and derivatives as heterogeneous Fenton-like catalysts for organic wastewater treatment: a review, Environ. Int. 146 (2021), 106273.

[30] C. Bao, H. Wang, C. Wang, X. Zhang, X. Zhao, C. Dong, Y. Huang, S. Chen, P. Guo, X. She, Y. Sun, D. Yang, Cooperation of oxygen vacancy and FeIII/FeII sites in H_2-reduced Fe-MIL-101 for enhanced Fenton-like degradation of organic pollutants, J. Hazard. Mater. 441 (2023), 129922.

[31] N. Li, G. Chen, J. Zhao, B. Yan, Z. Cheng, L. Meng, V. Chen, Self-cleaning PDA/ZIF-67@PP membrane for dye wastewater remediation with peroxymonosulfate and visible light activation, J. Membr. Sci. 591 (2019), 117341.

[32] I. Hod, M.D. Sampson, P. Deria, C.P. Kubiak, O.K. Farha, J.T. Hupp, Fe-porphyrin-based metal–organic framework films as high-surface concentration, heterogeneous catalysts for electrochemical reduction of CO_2, ACS Catal. 5 (2015) 6302–6309.

[33] Y. Shang, X. Duan, S. Wang, Q. Yue, B. Gao, X. Xu, Carbon-based single atom catalyst: synthesis, characterization, DFT calculations, Chin. Chem. Lett. 33 (2022) 663–673.

[34] Y. Shang, X. Xu, B. Gao, S. Wang, X. Duan, Single-atom catalysis in advanced oxidation processes for environmental remediation, Chem. Soc. Rev. 50 (2021) 5281–5322.

[35] C. Yang, S. Shang, Q. Gu, J. Shang, X.Y. Li, Metal-organic framework-derived carbon nanotubes with multi-active Fe-N/Fe sites as a bifunctional electrocatalyst for zinc-air battery, J. Energy Chem. 66 (2022) 306–313.

[36] W. Qu, C. Chen, Z. Tang, H. Wen, L. Hu, D. Xia, S. Tian, H. Zhao, C. He, D. Shu, Progress in metal-organic-framework-based single-atom catalysts for environmental remediation, Coord. Chem. Rev. 474 (2023), 214855.

[37] D.M. D'Alessandro, Exploiting redox activity in metal-organic frameworks: concepts, trends and perspectives, Chem. Commun. 52 (2016) 8957–8971.

[38] J. Hou, X. He, S. Zhang, J. Yu, M. Feng, X. Li, Recent advances in cobalt-activated sulfate radical-based advanced oxidation processes for water remediation: a review, Sci. Total. Environ. 770 (2021), 145311.

[39] L. Jin, S. You, N. Ren, B. Ding, Y. Liu, Mo vacancy-mediated activation of peroxymonosulfate for ultrafast micropollutant removal using an electrified MXene filter functionalized with Fe single atoms, Environ. Sci. Technol. 56 (2022) 11750–11759.

[40] Y. Chen, G. Zhang, H. Liu, J. Qu, Confining free radicals in close vicinity to contaminants enables ultrafast Fenton-like processes in the interspacing of MoS_2 membranes, Angew. Chem. Int. Ed. 58 (2019) 8134–8138.

[41] X. Wu, K. Rigby, D. Huang, T. Hedtke, X. Wang, M.W. Chung, S. Weon, E. Stavitski, J.H. Kim, Single-atom cobalt incorporated in a 2D graphene oxide membrane for catalytic pollutant degradation, Environ. Sci. Technol. 56 (2022) 1341–1351.

[42] S. Shang, C. Yang, C. Wang, J. Qin, Y. Li, Q. Gu, J. Shang, Transition-metal-containing porphyrin metal-organic frameworks as pi-backbonding adsorbents for NO_2 removal, Angew. Chem. Int. Ed. 59 (2020) 19680–19683.

[43] A. Fateeva, P.A. Chater, C.P. Ireland, A.A. Tahir, Y.Z. Khimyak, P.V. Wiper, J. R. Darwent, M.J. Rosseinsky, A water-stable porphyrin-based metal-organic framework active for visible-light photocatalysis, Angew. Chem. Int. Ed. 51 (2012) 7440–7444.

[44] P.W. Menezes, A. Indra, D. González-Flores, N.R. Sahraie, I. Zaharieva, M. Schwarze, P. Strasser, H. Dau, M. Driess, High-performance oxygen redox catalysis with multifunctional cobalt oxide nanochains: morphology-dependent activity, ACS Catal. 5 (2015) 2017–2027.

[45] R. Zhang, M. Tahir, S. Ding, M.A. Qadeer, H. Li, Q.-X. Zeng, R. Gao, L. Wang, X. Zhang, L. Pan, J.-J. Zou, Promotion of nitrogen reserve and electronic regulation in bamboo-like carbon tubules by cobalt nanoparticles for highly efficient ORR, ACS Appl. Energy Mater. 3 (2019) 2323–2330.

[46] A.N. Marianov, A.S. Kochubei, T. Roman, O.J. Conquest, C. Stampfl, Y. Jiang, Resolving deactivation pathways of Co porphyrin-based electrocatalysts for CO_2 reduction in aqueous medium, ACS Catal. 11 (2021) 3715–3729.

[47] J. Benner, T.A. Ternes, Ozonation of metoprolol: elucidation of oxidation pathways and major oxidation products, Environ. Sci. Technol. 43 (2009) 5472–5480.

[48] L. Liu, H. Mi, M. Zhang, F. Sun, R. Zhan, H. Zhao, S. He, L. Zhou, Efficient moxifloxacin degradation by $CoFe_2O_4$ magnetic nanoparticles activated peroxymonosulfate: kinetics, pathways and mechanisms, Chem. Eng. J. 407 (2021), 127201.

[49] X. Liang, D. Wang, Z. Zhao, T. Li, Y. Gao, C. Hu, Coordination number dependent catalytic activity of single-atom cobalt catalysts for fenton-like reaction, Adv. Funct. Mater. 32 (2022), 2203001.

[50] Y. Long, J. Dai, S. Zhao, Y. Su, Z. Wang, Z. Zhang, Atomically dispersed cobalt sites on graphene as efficient periodate activators for selective organic pollutant degradation, Environ. Sci. Technol. 55 (2021) 5357–5370.

[51] L. Peng, X. Duan, Y. Shang, B. Gao, X. Xu, Engineered carbon supported single iron atom sites and iron clusters from Fe-rich Enteromorpha for Fenton-like reactions via nonradical pathways, Appl. Catal. B Environ. 287 (2021), 119963.

[52] Y. Zhao, H. An, J. Feng, Y. Ren, J. Ma, Impact of crystal types of $AgFeO_2$ nanoparticles on the peroxymonosulfate activation in the water, Environ. Sci. Technol. 53 (2019) 4500–4510.

[53] C. Chu, J. Yang, X. Zhou, D. Huang, H. Qi, S. Weon, J. Li, M. Elimelech, A. Wang, J. H. Kim, Cobalt single atoms on tetrapyridomacrocyclic support for efficient peroxymonosulfate activation, Environ. Sci. Technol. 55 (2021) 1242–1250.

[54] X. Dong, Z. Gan, X. Lu, W. Jin, Y. Yu, M. Zhang, Study on catalytic and non-catalytic supercritical water oxidation of p-nitrophenol wastewater, Chem. Eng. J. 277 (2015) 30–39.

[55] C. Yang, Y. Fan, P. Li, Q. Gu, X.Y. Li, Freestanding 3-dimensional macro-porous SnO_2 electrodes for efficient electrochemical degradation of antibiotics in wastewater, Chem. Eng. J. 422 (2021), 130032.

[56] S. Zhang, V. Rouge, L. Gutierrez, J.P. Croue, Reactivity of chromophoric dissolved organic matter (CDOM) to sulfate radicals: Reaction kinetics and structural transformation, Water Res. 163 (2019), 114846.

[57] R. Makiura, S. Motoyama, Y. Umemura, H. Yamanaka, O. Sakata, H. Kitagawa, Surface nano-architecture of a metal-organic framework, Nat. Mater. 9 (2010) 565–571.

[58] Y. Wang, Z. Ao, H. Sun, X. Duan, S. Wang, Activation of peroxymonosulfate by carbonaceous oxygen groups: experimental and density functional theory calculations, Appl. Catal. B Environ. 198 (2016) 295–302.
[59] W.I. Dzik, X. Xu, X.P. Zhang, J.N. Reek, B. de Bruin, Carbene radicals' in CoII (por)-catalyzed olefin cyclopropanation, J. Am. Chem. Soc. 132 (2010) 10891–10902.
[60] C. Liu, V. Nanaboina, G.V. Korshin, W. Jiang, Spectroscopic study of degradation products of ciprofloxacin, norfloxacin and lomefloxacin formed in ozonated wastewater, Water Res. 46 (2012) 5235–5246.
[61] I. Ahmad, R. Bano, S.G. Musharraf, S. Ahmed, M.A. Sheraz, Q. ul Arfeen, M. S. Bhatti, Z. Shad, Photodegradation of moxifloxacin in aqueous and organic solvents: a kinetic study, AAPS PharmSciTech 15 (2014) 1588–1597.